mater.scichina.com link.springer.com

Sci China Mater 2025, 68(2): 464–471
https://doi.org/10.1007/s40843-024-3199-9

Evaluating the role of oxygen vacancies in CO_2 photothermal catalytic reduction to methanol over 2D Bi_2WO_6

Hong-Xia Fan[1*], Tao Liu[1], Liang-Fen Zhen[1], Antony Rajendran[2], Jie Feng[1] and Wen-Ying Li[1*]

ABSTRACT **Oxygen vacancies play a vital role in the adsorption, activation, and subsequent reduction of CO_2 to methanol. This work presents the preparation of two-dimensional Bi_2WO_6 nanosheets with different oxygen vacancy concentrations (BWO-OV1, BWO-OV2, and BWO-OV3) and the evaluation of their catalytic activity in the photothermal catalytic reduction of CO_2 to methanol. The oxygen vacancy concentration has played a decisive role in controlling the methanol yield. The BWO-OV2 catalyst with the highest oxygen vacancy concentration (13.9%) accomplishes the maximum methanol yield (82.45 μmol/(g h)). This is because the oxygen vacancies enhance the adsorption and activation of CO_2 in the form of CO_2^-, broaden the light adsorption range, and promote light-induced charge carrier separation. Also, BWO-OV2 exhibits 1.91 and 3.28 times higher catalytic activity in CO_2 reduction while being used under photothermal catalytic conditions than being employed under photocatalytic and thermal catalytic conditions, respectively. In line with the *in-situ* Fourier transform infrared spectroscopy and computational analysis, the external heat indiscriminately promotes the adsorption and further conversion of all involved intermediates but the light irradiation selectively enhances the adsorption of CO_2^-, HCOO*, and CH_3O* species. The findings of the present work might provide key mechanistic insights into understanding the role of thermal and light irradiation in photothermal catalysis.**

Keywords: Bi_2WO_6 catalysts, oxygen vacancy, photothermal catalysis, CO_2 reduction, methanol

INTRODUCTION

CO_2 conversion into value-added products, such as CO, CH_4, CH_3OH, HCOOH, and various C_{2+} hydrocarbons, is a sustainable solution to alleviate the energy crisis and environmental problems. Of particular importance, methanol (CH_3OH) can be substituted for oil and gas to generate a "methanol economy" and play an indispensable role in the future [1,2]. However, the thermodynamic and kinetic stability of CO_2 molecules with the higher C=O bond energy (750 kJ/mol) underlines the requirement of the enormous amount of energy input for their reduction even in the presence of a catalyst. The coupling of solar energy and thermal energy results in the effective regulation of activity and selectivity during CO_2 reduction [3]. For instance, Li *et al.* [4] prepared CuO and MgO composites by the hydrothermal method with different mass ratios and employed them as catalysts for the photothermal reduction of CO_2. The obtained methanol yield is 5.96 times higher than that of a thermal catalytic process. Li *et al.* [5] attained a liquid alcohol production rate of 7.45 μmol/(g h) during CO_2 reduction under photothermal conditions using a novel Bi_4TaO_8Cl/Bi heterojunction possessing oxygen vacancies (OVs). Intriguingly, photothermal catalysis not only combines the advantages of photocatalysis and thermal catalysis but also benefits from the synergistic effect of the two reactions to accelerate CO_2 reduction under mild conditions [6]. However, the success of photothermal CO_2 reduction lies in designing efficient stable catalysts and investigating reaction mechanisms [7,8]. Those catalysts should possess excellent light absorption capacity in addition to efficient charge carrier transfer and separation. Besides, they should demonstrate a better CO_2 adsorption and activation capacity [9]. However, photocatalytic CO_2 reduction to methanol remains challenging as it demands multiple electrons and protons to break the C=O bond and form new bonds. This underlines the necessity of efficient and selective photothermal catalysts for CO_2 reduction to methanol.

Bi_2WO_6 (BWO) is one of the simplest Aurivillius oxides made up of alternately stacked $[Bi_2O_2]^{2+}$ and octahedral $[WO_4]^{2-}$ layers that facilitate the separation of photogenerated carriers. Favorably, it is photoresponsive ranging from visible to ultraviolet (UV) light, and stable under light irradiation and heat, besides being environmentally benign [10,11]. These properties of BWO underline its broad prospects in photothermal catalytic CO_2 reduction. However, the limitations like a less photogenerated carrier separation efficiency and the availability of insufficient surface-active sites hamper the practical application of BWO in CO_2 reduction. To tackle these issues, many strategies have been attempted, such as designing heterojunction [12], element doping [13], and introducing OVs [14]. The morphology of BWO photocatalysts also plays a key role in enriching surface active sites and reducing charge transfer pathways. Importantly, OVs optimize the electronic structure to afford higher charge mobility [15,16] in addition to increasing light absorption and CO_2 activation, as evidenced by the literature [17,18]. Hence, the catalysts having a special morphology and OVs have become popular. Bi_2MoO_6, a similar catalyst to BWO, exhibits a unique layered Aurivillius structure [19]. Huang *et al.* [20] fabricated the atomically thin Bi_2MoO_6 nanosheets with OVs by wet chemical synthesis to reach the improved photocatalytic degradation of phenol with good cycling stability.

[1] State Key Laboratory of Clean and Efficient Coal Utilization, Taiyuan University of Technology, Taiyuan 030024, China
[2] Department of Chemistry, Mepco Schlenk Engineering College (Autonomous), Sivakasi 626005, Tamil Nadu, India
* Corresponding author (email: fanhongxia@tyut.edu.cn; ying@tyut.edu.cn)

Therefore, the combination of a two-dimensional (2D) structure and OVs in BWO is expected to show a synergistic effect in the photothermal CO_2 reduction. However, the insight into the role of OVs in photothermal catalysis remains unclear.

Based on the above facts, 2D BWO has been prepared with different OV concentrations and employed as catalysts in photothermal CO_2 reduction after being characterized. The possible catalytic mechanism and the role of coupling light irradiation with heat in photothermal CO_2 reduction to methanol have been proposed using *in-situ* Fourier transform infrared (FT-IR) spectroscopy and theoretical analysis.

EXPERIMENTAL SECTION

Catalyst preparation

2D BWO nanosheets with different OV concentrations were prepared under hydrothermal conditions followed by heat treatment in a hydrogen-argon atmosphere using $Bi(NO_3)_3 \cdot 5H_2O$, $Na_2WO_4 \cdot 2H_2O$, hexadecyl trimethyl ammonium bromide (CTAB), and ultrapure water. The detailed experimental procedure is provided in the Supplementary information. The absence of CTAB is ensured in the final catalysts according to the FT-IR spectra (Fig. S1).

CO_2 photothermal catalytic reduction

The photothermal catalytic CO_2 reduction to methanol was carried out in a reactor (NSV-50-316 L, Anhui Kemi Instrument Co., Ltd.) under a 300 W xenon lamp (Beijing Zhongjiao Jinyuan Technology Co., Ltd.), the light source, coupled with 300 nm cut off filter. The reaction products were analyzed by gas chromatography (Agilent 8890). The experimental details are provided in the Supplementary information.

In-situ FT-IR spectroscopy

In-situ FT-IR experiments were performed on a Bruker TENSOR 27 infrared spectrometer. The details are discussed in the Supplementary information.

RESULTS AND DISCUSSION

Catalyst characterization

The typical preparation of BWO with different OV concentrations is schematically illustrated in Fig. 1a. The morphology and textural properties of catalysts are characterized by scanning electron microscopy (SEM) and transmission electron microscopy (TEM). Fig. 1b and Fig. S2 indicate that the CTAB-assisted synthesis of BWO leads to a 2D nanosheet morphology. The ultrathin nature of nanosheets is confirmed by atomic force microscopy (AFM) image of BWO. The corresponding height cutaway view displays the thickness of BWO nanosheets is approximately 1.58 nm (Fig. 1c). The lattice spacing (0.272 nm) matches with the (020) planes of BWO and suggests the the growth of 2D BWO nanosheet in the (001) direction (Fig. 1d, e) [21].

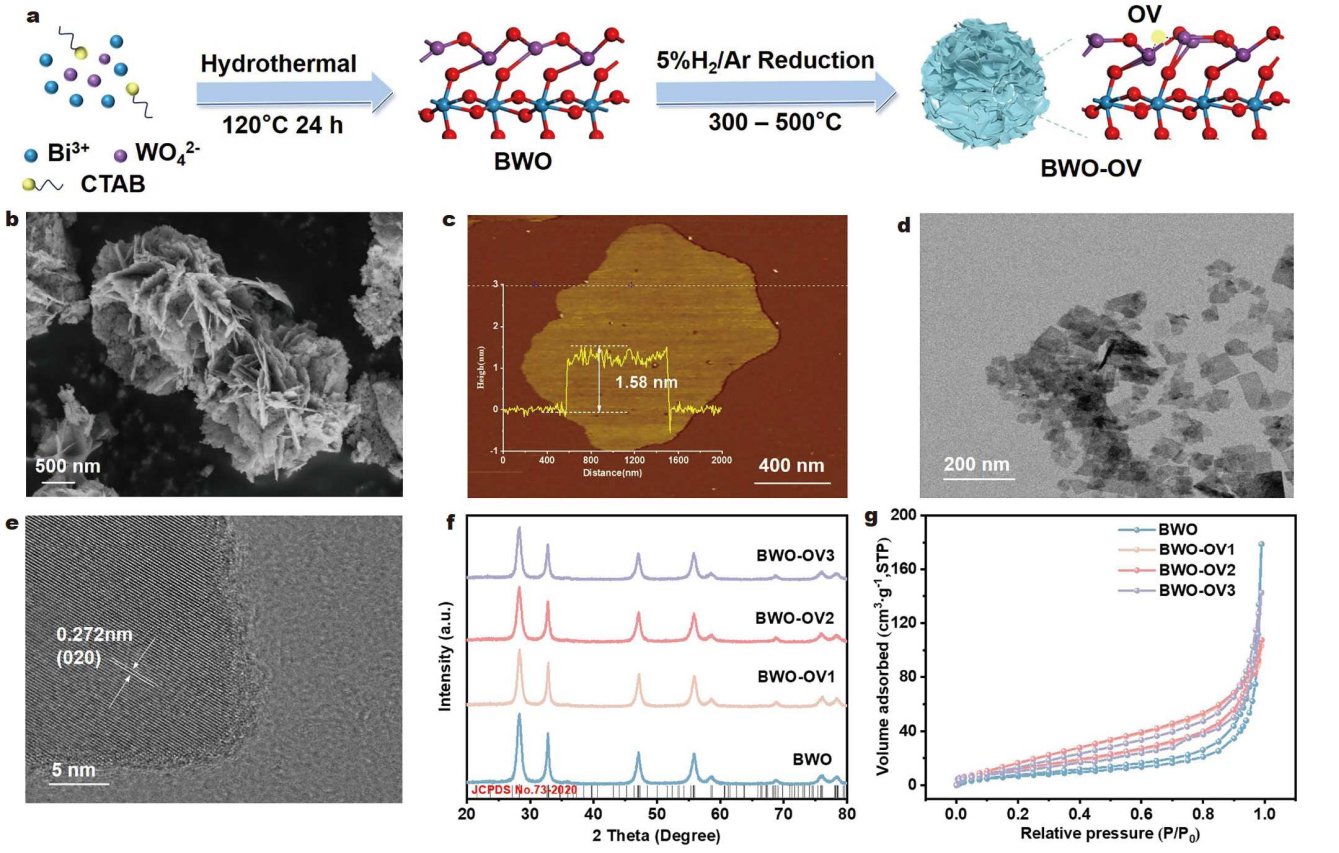

Figure 1 (a) Schematic showing the preparation of ultrathin BWO and BWO-OV nanosheets. (b) SEM image of BWO-OV2. (c) AFM image and height profiles of BWO-OV2. (d, e) TEM images of BWO-OV2. (f) XRD patterns of different BWO samples. (g) Nitrogen adsorption-desorption isotherms of BWO samples.

The crystal structure of the BWO catalyst is characterized by X-ray diffraction (XRD). Fig. 1f illustrates that all prepared BWO samples show diffraction peaks at 28.3°, 32.8°, 47.1°, and 55.8° corresponding to (113), (020), (220) and (313) crystal planes, respectively, according to the JCPDS data of BWO (JCPDS No. 73-2020) [22]. The similarity between the XRD patterns of the original BWO and BWO-OV indicates that the heat treatment under a hydrogen atmosphere does not have a significant impact on the crystal structure of BWO.

Fig. 1g shows the N_2 adsorption-desorption isotherms of prepared catalysts. They follow type IV isotherm with type H3 hysteresis loops, indicating the formation of BWO with narrow pores attributed to the flaky morphology [23]. Brunauer-Emmett-Teller (BET)-specific surface areas of BWO, BWO-OV1, BWO-OV2, and BWO-OV3 are 28.3, 50.4, 48.6, and 40.5 m^2/g, respectively.

OVs and their concentrations in the prepared BWO catalysts are analyzed by X-ray photoelectron spectroscopy (XPS) and electron paramagnetic resonance (EPR) spectra. The full XPS spectrum displays the peaks of Bi, W, and O elements (Fig. S3). Based on the high-resolution Bi 4f spectrum of BWO (Fig. 2a), peaks at 164.52 and 159.20 eV are attributed to Bi $4f_{7/2}$ and Bi $4f_{5/2}$ spin-orbit splitting photoelectron levels of Bi^{3+} chemical state, respectively. Compared with the original BWO, the Bi 4f peaks shift to the higher binding energy due to the heat treatment done in the hydrogen atmosphere. This implies the generation of OV adjacent to Bi atoms, intriguingly, with a higher electron-withdrawing ability [14]. In Fig. 2b, the distinctive peaks of W 4f appear at 35.48 eV (W $4f_{7/2}$) and 37.65 eV (W $4f_{5/2}$). These peaks are also shifted due to the heat treatment carried in the hydrogen atmosphere, which is assigned to the change in electron density after OV generation. The two O 1s peaks observed at 530.0 and 531.6 eV correspond to lattice and surface-adsorbed oxygen, respectively (Fig. 2c) [24]. For the original BWO, the OVs proportion in O 1s is 5.6% according to the peak area. It is found to increase in the BWO-OV catalysts, i.e., 10.3% (BWO-OV1), 13.9% (BWO-OV2), and 9.3% (BWO-OV3). Thus, the order of OV concentration in the prepared catalysts is BWO-OV2 > BWO-OV1 > BWO-OV3 > BWO.

The presence of OVs in all the prepared catalysts is also confirmed by the appearance of a sharp EPR signal centered at g = 2.003 due to the unpaired electrons trapped at OV sites (Fig. 2d). The peak intensity of this EPR signal can be related to the concentration of OVs in the sample [25,26]. Thus, according to the peak intensity of the EPR signal, the order of OV concentration in the prepared catalysts follows the same trend as supported by XPS analysis.

Photothermal catalytic reduction of CO_2 to methanol

The catalytic performance of the prepared catalysts is evaluated by combining external heating (30–120°C) and UV light (300 nm) in a stainless-steel reactor (Fig. S4) using gaseous CO_2 and liquid H_2O. Fig. 3a displays that the methanol yield is directly proportional to the concentration of OVs available in the catalysts. Accordingly, the methanol yield obtained with our catalysts follows a trend as BWO-OV2 > BWO-OV1 > BWO-OV3 > BWO. BWO-OV2 with a higher OV concentration (13.9%) demonstrates the best catalytic activity with a methanol yield of 82.45 μmol/(g h).

To evaluate the effect of external heating temperature, an infrared imager is used to test the temperature change. The possible increase in temperature due to the light irradiation is excluded (Fig. S5). The catalytic activity of BWO-OV2 increases while increasing the external heating temperature up to 90°C but

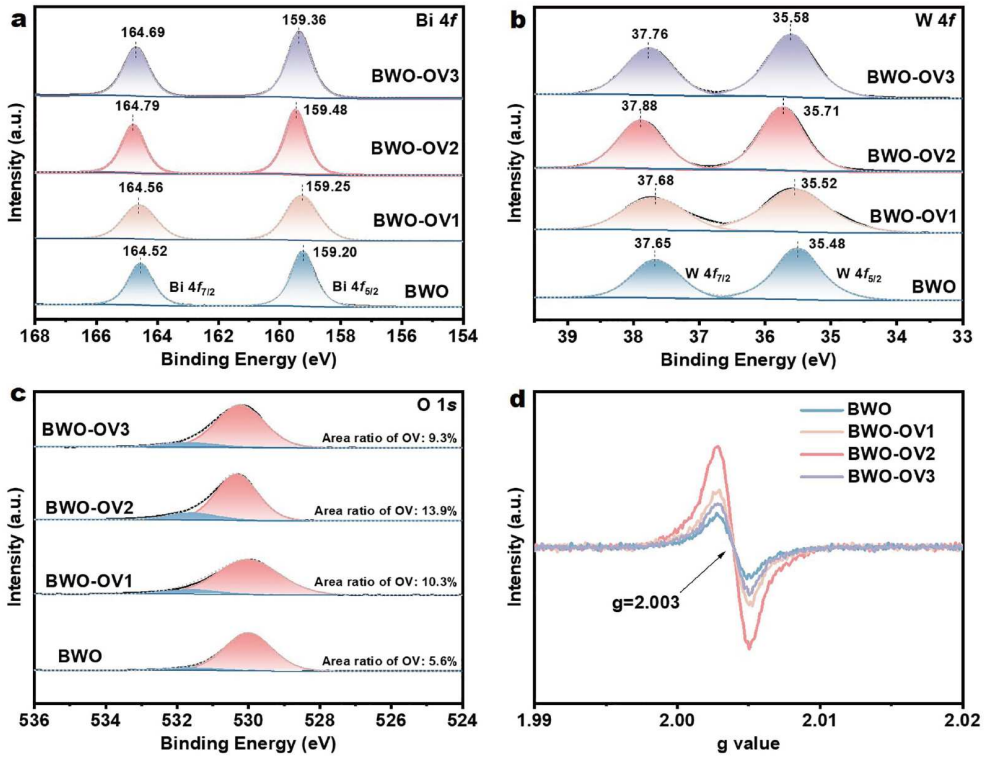

Figure 2 XPS spectra of the prepared catalysts. (a) Bi 4f, (b) W 4f, (c) O 1s, and (d) EPR spectra of the prepared catalysts.

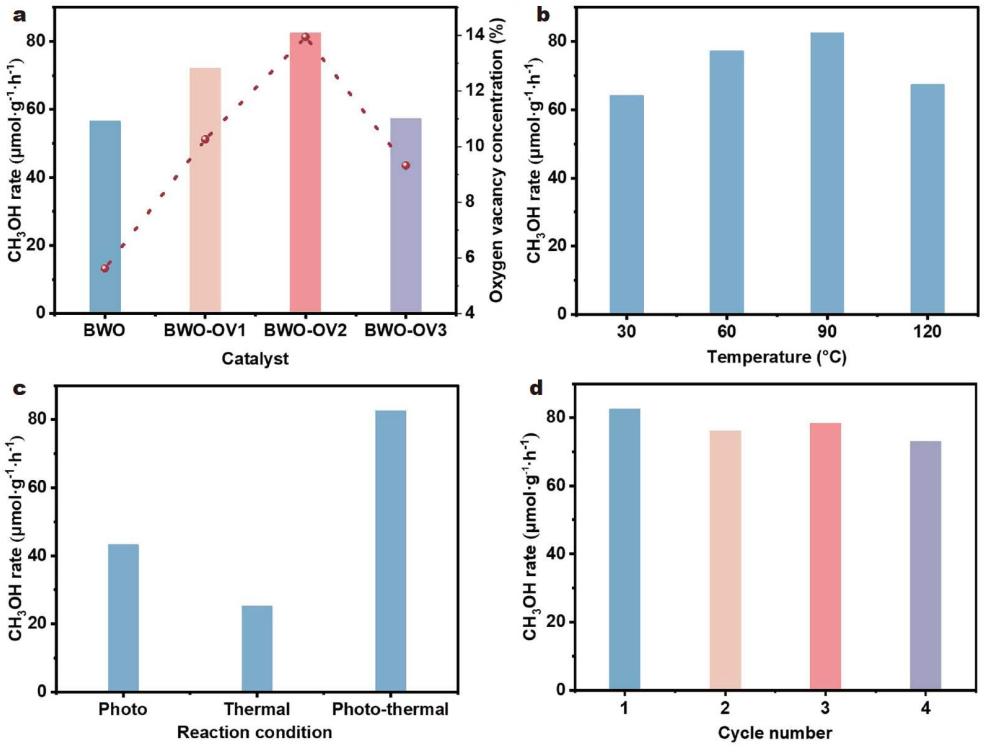

Figure 3 Catalytic performance under different experimental conditions. (a) Photothermal catalytic CO_2 reduction (light irradiation λ = 300 nm, 90°C) using the prepared catalysts. (b) Photothermal catalytic CO_2 reduction using BWO-OV2 at various external heating temperatures (30–90°C). (c) Photocatalytic (light irradiation λ = 300 nm, 25°C), thermal catalytic (90°C), and photothermal catalytic (light irradiation λ = 300 nm, 90°C) conditions. The other reaction conditions followed uniformly in the above reactions: initial CO_2 pressure of 1 MPa, 20 mL H_2O, 300 W xenon lamp, irradiation time of 4 h. (d) Catalyst reusability.

decreases with further increase in temperature (Fig. 3b). The obtained methanol yield under photothermal conditions at 90°C is 1.91 and 3.28 times than that under photocatalytic and thermal catalytic conditions, respectively (Fig. 3c). Moreover, the activity of BWO-OV2 at room temperature (RT) is increased 20.69 times than that under UV irradiation (Fig. S6). These results reveal that light irradiation makes a major contribution to the photothermal catalytic reduction of CO_2 as compared to external heating temperature. The stability of BWO-OV2 was evaluated by performing the catalyst reusability experiment. The CH_3OH yield reaches 88.45% even during the 4th catalytic cycle, indicating the good stability of BWO-OV2 (Fig. 3d).

No significant change is noticed in the structure and morphology of spent BWO-OV2 in line with the XRD pattern and SEM image. This underlines the structural integrity of the catalyst under photothermal conditions (Figs S7 and S8).

Optical and optoelectronic properties

The optical and photoelectronic properties of the catalysts are observed to determine the origin of the increase in catalytic activity caused by OVs.

As shown in Fig. 4a, UV-Vis spectra of all the catalysts show an obvious absorption band in the UV region. The bandgap widths calculated for BWO, BWO-OV1, BWO-OV2, and BWO-OV3 are 2.76, 1.24, 1.40, and 2.32 eV, respectively (Fig. S9). The band gap of the BWO-OV catalysts is narrower than that of BWO. The catalysts with more OVs broaden the optical response range to the visible region, manifesting that OVs enable a wide light response range. Hence, visible light with a low energy can also excite photogenerated carriers.

Photoluminescence (PL) spectra and the photoelectrochemical response of prepared catalysts are studied to explore the electron and hole migration and separation capacity. The weaker PL intensity reflects the lower degree of electron-hole recombination. Increasing the concentration of OVs in BWO achieves a better inhibition of the electron-hole recombination (Fig. 4b). The transient photocurrent response tests under xenon lamp irradiation further illustrate the behavior of charge carriers. The spectra of BWO-OV catalysts display significantly increased photocurrent density as compared to BWO (Fig. 4, Fig. S10), indicating the effective separation of photogenerated carriers.

Fig. 4c reveals that the trend in the Nyquist arc radius is as follows: BWO > BWO-OV3 > BWO-OV1 > BWO-OV2. The increase in arc radius with the increase of OVs in the catalysts enables the lower charge transfer resistance and thus facilitates the charge separation [27].

Therefore, enriching OVs in the catalysts improves the light adsorption and photogenerated electrons, which might be due to the facile capture of photogenerated electrons by OVs [28]. As a consequence, the possibility of photogenerated electrons and hole recombination is reduced with the fact that OVs can offer sufficient electrons for CO_2 activation.

In-situ FT-IR spectroscopy

To gain molecular-level insights into the increase of catalytic superior activity due to the enrichment of OVs and to distinguish the impact of external heat and light irradiation, CO_2 adsorption and subsequent reaction are examined by CO_2-

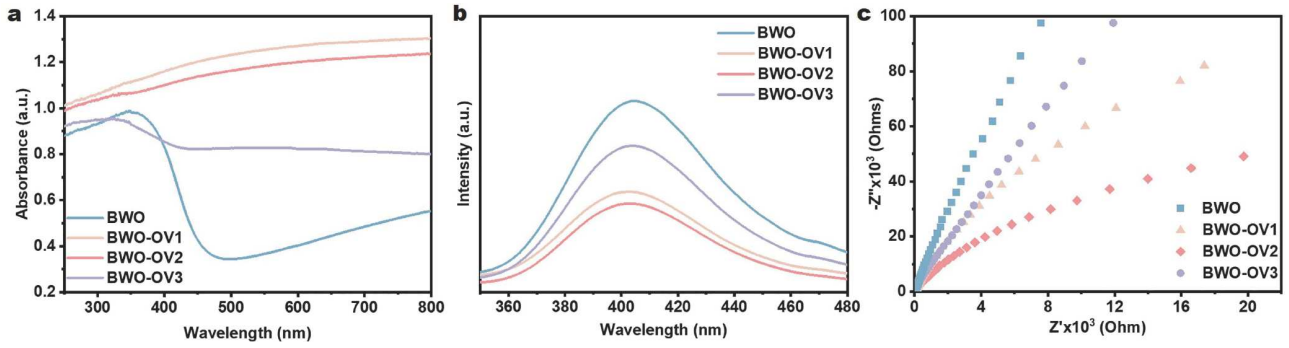

Figure 4 Optical and electronic properties of the prepared catalysts. (a) UV-Vis spectra, (b) PL spectra, and (c) electrochemical impedance spectroscopy (EIS) Nyquist plots.

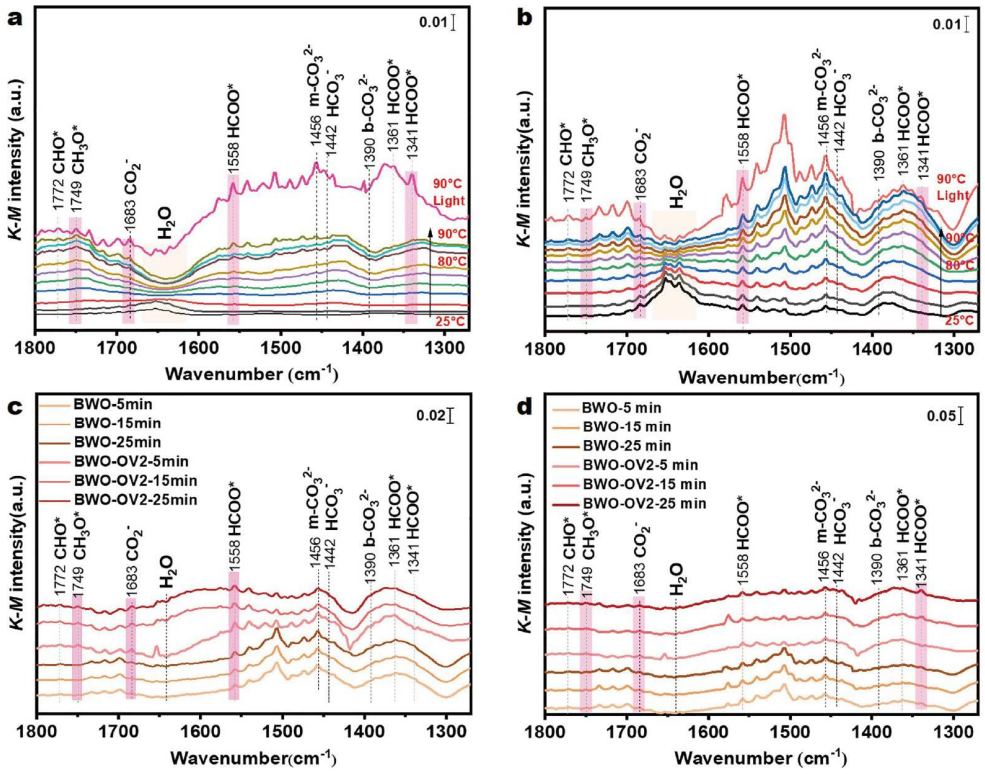

Figure 5 *In-situ* FT-IR spectra of (a) BWO-OV2 and (b) BWO under thermal and photothermal catalytic conditions. BWO and BWO-OV2 (c) under thermal and (d) photothermal catalytic conditions.

temperature-programmed desorption (TPD) and *in-situ* FT-IR under different conditions.

Under thermal catalytic conditions, the CO_2-TPD of BWO and BWO-OV2 catalysts are evaluated. The signals of CO_2 desorption shift to high temperatures with increasing OV concentration (Fig. S11). This is assigned to the improvement of interaction between CO_2 and BWO. In the *in-situ* FT-IR spectrum of BWO-OV2 (Fig. 5a), the intensity of the peak at 1640 cm^{-1} decreases (the bending and stretching vibrations of O–H bonds of absorbed H_2O) [29]. In contrast, the intensity of the characteristic peaks of intermediates (HCO_3^- (1442 cm^{-1}), b-CO_3^{2-} (1390 cm^{-1}), m-CO_3^{2-} (1456 cm^{-1}), CO_2^- (1683 cm^{-1}), HCOO* (1558, 1361 and 1341 cm^{-1}), and CH_3O* (1749 cm^{-1})) increase with temperature [30–33]. However, the peak intensity barely changed over the prolonged time. A similar behavior is also observed in BWO (Fig. 5b).

After applying light irradiation (λ = 200–400 nm), the peak intensity of CO_2^-, HCOO*, and CH_3O* is remarkably increased (Fig. 5a). These results reveal that the external heat indiscriminately promotes the adsorption of all involved intermediates but light irradiation selectively enhances the adsorption of CO_2^-, HCOO*, and CH_3O* species.

Moreover, the intensity of the above-mentioned intermediates is compared for BWO and BWO-OV2 to determine the role of OVs in CO_2 photothermal catalytic reduction. As shown in Fig. 5c, d, in both the thermal and photothermal catalytic conditions, BWO-OV2 exhibits a higher intensity for CO_2^-, HCOO*, and CH_3O* as compared to BWO. The corresponding peaks of these three species are remarkably strengthened over a prolonged time. Thus, it is obvious that the existence of OVs

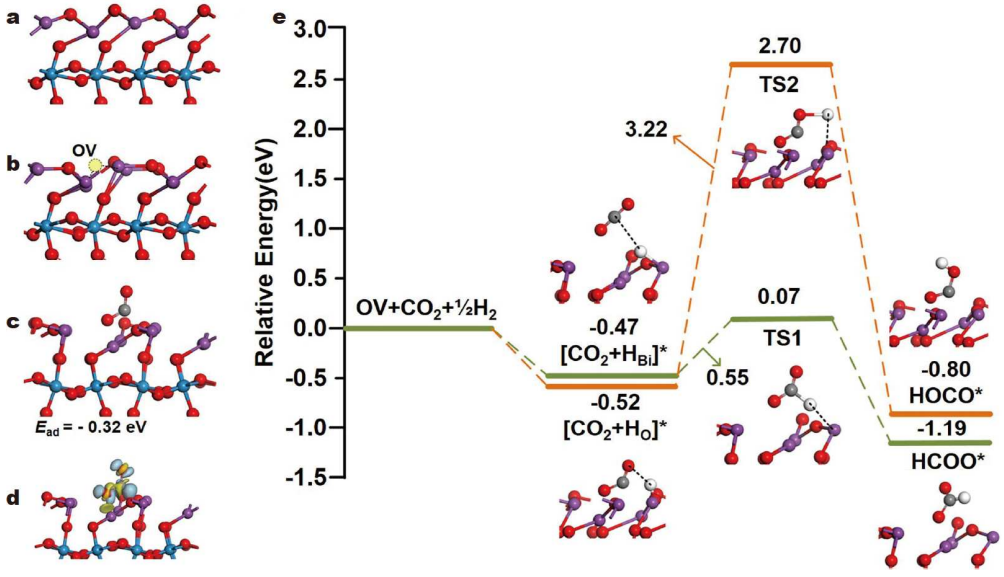

Figure 6 Configurations of (a) BWO (001), (b) BWO (001)-OV, and (c) CO_2 adsorption on BWO (001)-OV and (d) corresponding isosurface patterns of the electron density difference with the surface value of ±0.05 eV/Å. (e) Potential energy profile of CO_2 hydrogenation to HCOO* and HOCO* on the BWO (001)-OV obtained by DFT calculations.

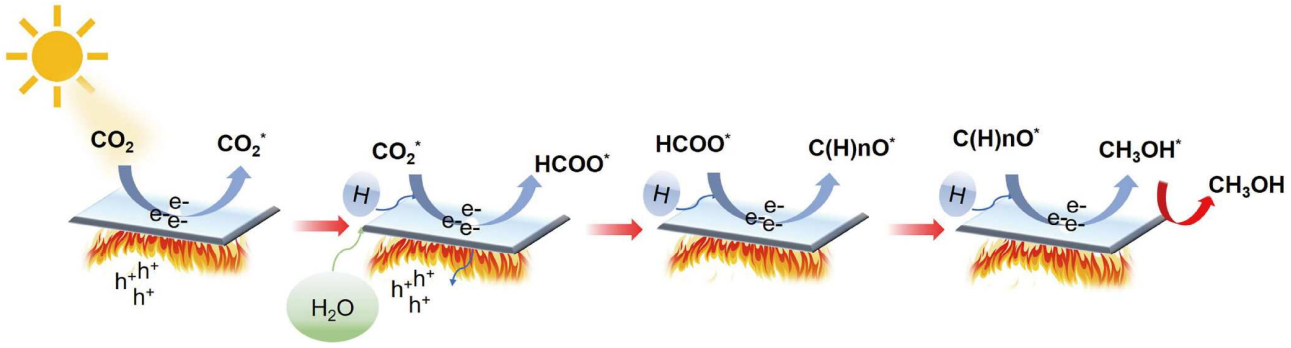

Scheme 1 Reaction pathway for CO_2 reduction to CH_3OH by the photothermal catalytic process.

improves the adsorption of CO_2^-, HCOO*, and CH_3O*, regardless of the thermal or photothermal catalytic process. The light irradiation provides more electrons for the surface reaction and gaseous CO_2 is mainly adsorbed on the catalysts surface in the form of CO_2^-, which is then hydrogenated to HCOO*, and further to CH_3O*.

To further confirm the mechanism, first-principles density functional theory (DFT) calculation is performed on the BWO (001) surface with OVs to observe the CO_2 adsorption and subsequent hydrogenation. The calculation models are created (Fig. 6a, b) based on TEM images. Fig. 6c, d exhibit the favorable adsorption configuration of CO_2, i.e., the insertion of one of the O atoms into the OV site of BWO (001) and the formation of bent CO_2^- species with the electron donation from the OV site [34,35]. The adsorbed CO_2 is kinetically and thermodynamically hydrogenated to HCOO* than to HOCO* with a lower activation barrier of 0.55 eV and exothermicity of 0.72 eV (Fig. 6e).

Based on the above results, a possible mechanism for the photothermal catalytic CO_2 reduction to methanol is proposed (Scheme 1). The CO_2 molecule is initially adsorbed on the catalyst surface to form CO_2^-. Then, the photogenerated holes oxidize the H_2O molecules, providing the necessary proton to react with CO_2^- to form HCOO*, i.e., the so-called formate pathway. This intermediate is converted to CH_3O* intermediate due to photogenerated electrons and H protons, and finally, methanol is generated.

CONCLUSIONS

2D BWO nanosheets with different OV concentrations have been fabricated by a facile hydrothermal method followed by hydrogen-assisted heat treatment for photothermal catalytic CO_2 reduction to methanol. Owing to the abundant actives, BWO-OV2 nanosheets have shown the highest methanol yield (82.45 μmol/(g h)) in CO_2 reduction, as compared to other BWO catalysts. The ultrathin morphology and the presence of OVs in higher concentrations play a crucial role in the enhanced catalytic performance. XPS analysis, transient photocurrent response, and EIS Nyquist plots suggest that the concentration of OVs and the effective separation of photogenerated carriers (holes and electrons) are the reasons behind the improved catalytic activity. Additionally, *in-situ* FT-IR combined with DFT calculations reveal that the adsorbed CO_2 molecule is initially converted to CO_2^- and then transferred to HCOO*. Thermal energy increases the transfer rate of reactants and thus enhances

the reaction kinetics. Light irradiation does not alter the reaction pathways but significantly promotes the activation and conversion of HCOO* intermediates, thereby facilitating methanol production. The OVs in BWO can optimize the photothermal catalytic CO_2 reduction and open new possibilities for CO_2 reduction driven by high-performance solar energy.

Received 9 October 2024; accepted 21 November 2024; published online 2 January 2025

1 Olah GA. Beyond oil and gas: the methanol economy. Angew Chem Int Ed, 2005, 44: 2636–2639
2 Ren M, Zhang Y, Wang X, *et al.* Catalytic hydrogenation of CO_2 to methanol: a review. Catalysts, 2022, 12: 403
3 Wang Z, Song H, Liu H, *et al.* Coupling of solar energy and thermal energy for carbon dioxide reduction: status and prospects. Angew Chem Int Ed, 2020, 59: 8016–8035
4 Li T, Guo H, Wang X, *et al.* Loading CuO on the surface of MgO with low-coordination basic O^{2-} sites for effective enhanced CO_2 capture and photothermal synergistic catalytic reduction of CO_2 to ethanol. Chin J Chem Eng, 2023, 61: 58–67
5 Li S, Wang C, Li D, *et al.* Bi_4TaO_8Cl/Bi heterojunction enables high-selectivity photothermal catalytic conversion of CO_2-H_2O flow to liquid alcohol. Chem Eng J, 2022, 435: 135133
6 Tang Y, Yang Z, Guo C, *et al.* Encapsulating Ir nanoparticles into UiO-66 for photo-thermal catalytic CO_2 methanation under ambient pressure. J Mater Chem A, 2022, 10: 12157–12167
7 Tian J, Han R, Guo Q, *et al.* Direct conversion of CO_2 into hydrocarbon solar fuels by a synergistic photothermal catalysis. Catalysts, 2022, 12: 612
8 Wang Z, Yang Z, Fang R, *et al.* A state-of-the-art review on action mechanism of photothermal catalytic reduction of CO_2 in full solar spectrum. Chem Eng J, 2022, 429: 132322
9 Fang S, Hu YH. Thermo-photo catalysis: a whole greater than the sum of its parts. Chem Soc Rev, 2022, 51: 3609–3647
10 Chen T, Liu L, Hu C, *et al.* Recent advances on Bi_2WO_6-based photocatalysts for environmental and energy applications. Chin J Catal, 2021, 42: 1413–1438
11 Zhong X, Liu Y, Hou T, *et al.* Effect of Bi_2WO_6 nanoflowers on the U(VI) removal from water: roles of adsorption and photoreduction. J Environ Chem Eng, 2022, 10: 107170
12 Zhu Y, Wang Y, Ling Q, *et al.* Enhancement of full-spectrum photocatalytic activity over $BiPO_4$/Bi_2WO_6 composites. Appl Catal B-Environ, 2017, 200: 222–229
13 Zhang Z, Wang W, Gao E, *et al.* Enhanced photocatalytic activity of Bi_2WO_6 with oxygen vacancies by zirconium doping. J Hazard Mater, 2011, 196: 255–262
14 Kong XY, Choo YY, Chai SP, *et al.* Oxygen vacancy induced Bi_2WO_6 for the realization of photocatalytic CO_2 reduction over the full solar spectrum: from the UV to the NIR region. Chem Commun, 2016, 52: 14242–14245
15 Wu X, Ling Tan H, Zhang C, *et al.* Recent advances in two-dimensional ultrathin Bi-based photocatalysts. Prog Mater Sci, 2023, 133: 101047
16 Li B, Shao L, Wang R, *et al.* Interfacial synergism of Pd-decorated BiOCl ultrathin nanosheets for the selective oxidation of aromatic alcohols. J Mater Chem A, 2018, 6: 6344–6355
17 Liu T, Li H, Gao J, *et al.* Effect of oxygen vacancies on the photocatalytic CO_2 reduction performance of Bi_2WO_6: DFT and experimental studies. Appl Surf Sci, 2022, 579: 152135
18 Zhang Q, Yang P, Zhang H, *et al.* Oxygen vacancies in Co_3O_4 promote CO_2 photoreduction. Appl Catal B-Environ, 2022, 300: 120729
19 Kumar A, Singh P, Khan AAP, *et al.* CO_2 photoreduction into solar fuels via vacancy engineered bismuth-based photocatalysts: selectivity and mechanistic insights. Chem Eng J, 2022, 439: 135563
20 Huang Y, Li K, Li S, *et al.* Ultrathin Bi_2MoO_6 nanosheets for photocatalysis: performance enhancement by atomic interfacial engineering. ChemistrySelect, 2018, 3: 7423–7428
21 Sun D, Le Y, Jiang C, *et al.* Ultrathin Bi_2WO_6 nanosheet decorated with Pt nanoparticles for efficient formaldehyde removal at room temperature. Appl Surf Sci, 2018, 441: 429–437
22 Feng Y, Zhang Z, Zhao K, *et al.* Photocatalytic nitrogen fixation: oxygen vacancy modified novel micro-nanosheet structure $Bi_2O_2CO_3$ with band gap engineering. J Colloid Interface Sci, 2021, 583: 499–509
23 Li H, Zhang J, Yu J, *et al.* Ultra-thin carbon-doped Bi_2WO_6 Nanosheets for enhanced photocatalytic CO_2 reduction. Trans Tianjin Univ, 2021, 27: 338–347
24 Wang Y, Chen T, Chen F, *et al.* Metal-induced oxygen vacancies on Bi_2WO_6 for efficient CO_2 photoreduction. Sci China Mater, 2022, 65: 3497–3503
25 Wang J, Liang H, Zhang C, *et al.* Bi_2WO_{6-x} nanosheets with tunable Bi quantum dots and oxygen vacancies for photocatalytic selective oxidation of alcohols. Appl Catal B-Environ, 2019, 256: 117874
26 Huo WC, Dong X, Li JY, *et al.* Synthesis of Bi_2WO_6 with gradient oxygen vacancies for highly photocatalytic NO oxidation and mechanism study. Chem Eng J, 2019, 361: 129–138
27 Zhang X, Yu L, Zhuang C, *et al.* Highly asymmetric phthalocyanine as a sensitizer of graphitic carbon nitride for extremely efficient photocatalytic H_2 production under near-infrared light. ACS Catal, 2014, 4: 162–170
28 Xie J, Lu Z, Feng Y, *et al.* A small organic molecule strategy for remedying oxygen vacancies by bismuth defects in BiOBr nanosheet with excellent photocatalytic CO_2 reduction. Nano Res, 2024, 17: 297–306
29 Yan K, Chen L, Hu Y, *et al.* Accelerating solar driven CO_2 reduction via sulfur-doping boosted water dissociation and proton transfer. Nano Res, 2024, 17: 1056–1065
30 Li Z, Zhu G, Zhang W, *et al.* Dual-functional copper (Cu^0/Cu^{2+})-modified $SrTiO_{3-\delta}$ nanosheets with enhanced photothermal catalytic performance for CO_2 reduction and H_2 evolution. Chem Eng J, 2023, 452: 139378
31 Wang JC, Qiao X, Shi W, *et al.* Enhanced photothermal selective conversion of CO_2 to CH_4 in water vapor over rod-like Cu and N co-doped TiO_2. Chin J Struct Chem, 2022, 41: 2212033–2212042
32 Guo C, Tang Y, Yang Z, *et al.* Reinforcing the efficiency of photothermal catalytic CO_2 methanation through integration of Ru nanoparticles with photothermal $MnCo_2O_4$ nanosheets. ACS Nano, 2023, 17: 23761–23771
33 Jia Z, Ning S, Tong Y, *et al.* Selective photothermal reduction of CO_2 to CO over Ni-nanoparticle/N-doped CeO_2 nanocomposite catalysts. ACS Appl Nano Mater, 2021, 4: 10485–10494
34 Lei B, Cui W, Chen P, *et al.* C–doping induced oxygen-vacancy in WO_3 nanosheets for CO_2 activation and photoreduction. ACS Catal, 2022, 12: 9670–9678
35 Wang M, Shen M, Jin X, *et al.* Oxygen vacancy generation and stabilization in CeO_{2-x} by Cu introduction with improved CO_2 photocatalytic reduction activity. ACS Catal, 2019, 9: 4573–4581

Acknowledgement This work was supported by the National Key R&D Program of China (2022YFE0208400), the National Natural Science Foundation of China (U22A20211 and 22308248), and the Fundamental Research Funds for the Central Universities (2022ZFJH04).

Author contributions Li WY and Fan HX conceived the project and designed the experiments. Liu T and Zhen LF performed the experiments and analyzed the data. Fan HX, Liu T, and Zhen LF wrote the manuscript together. All authors discussed the results and reviewed the manuscript.

Conflict of interest The authors declare that they have no conflict of interest.

Supplementary information Supplementary materials are available in the online version of the paper.

Hong-Xia Fan is currently an associate professor at Taiyuan University of Technology (TYUT). She received her PhD degree (2017) from TYUT. During her PhD studies, she worked in Prof. Qingfeng Ge's group, Southern Illinois University, Carbondale, USA, as a jointly training doctor (1 year). Subsequently, she joined Prof. Wenying Li's research group. Her research interests are the design and preparation of catalysts for CO_2 utilization, oxidative dehydrogenation of hydrocarbons, and refining of coal liquefaction oil.

Wen-Ying Li is the director of the State Key Laboratory of Clean and Efficient Coal Utilization, TYUT and the Distinguished Professor of "Cheung Kong Scholars Program" in 2010. Her current research focuses entirely on enabling discovery and design of processes and catalysts for sustainable energy.

2D Bi_2WO_6表面氧空位在光热催化CO_2还原制甲醇反应中的作用

范鸿霞[1*], 刘涛[1], 甄良芬[1], Antony Rajendran[2], 冯杰[1], 李文英[1*]

摘要 氧空位在CO_2吸附、活化以及还原制甲醇过程中至关重要. 本研究制备了3种具有不同氧空位浓度的二维Bi_2WO_6纳米片用于光热催化CO_2还原制甲醇, 分别是BWO-OV1, BWO-OV2与BWO-OV3. 在90°C和300 nm光照条件下, 以甲醇产率为考核指标, 结果显示, 反应4 h后甲醇产率与氧空位浓度呈正相关, 氧空位浓度为13.9%的BWO-OV2甲醇产率达82.45 μmol/(g h), 分别是单独300 nm光照、90°C条件下的1.91和3.28倍. 原位红外表征分析表明, Bi_2WO_6表面氧空位不仅可以促进CO_2以CO_2^-形式发生吸附活化, 还可以拓宽光吸收范围及促进光生载流子分离. 90°C反应温度可以促进反应涉及全部中间体的吸附, 光照作用在于选择性增强CO_2^-、HCOO*和CH_3O*的吸附, 更有利于甲醇生成. 本研究及获得结果信息为理解光热催化反应中热与光照的作用提供了新见解.